

Excitation and scattering of surface plasmon-polaritons on structured metal films and their application to pulse shaping and enhanced transmission

This article has been downloaded from IOPscience. Please scroll down to see the full text article.

2005 New J. Phys. 7 249

(<http://iopscience.iop.org/1367-2630/7/1/249>)

View [the table of contents for this issue](#), or go to the [journal homepage](#) for more

Download details:

IP Address: 38.107.179.212

The article was downloaded on 20/02/2012 at 22:21

Please note that [terms and conditions apply](#).

Excitation and scattering of surface plasmon-polaritons on structured metal films and their application to pulse shaping and enhanced transmission

Amit Agrawal, Hua Cao and Ajay Nahata¹

Department of Electrical and Computer Engineering, University of Utah,
Salt Lake City, UT 84112, USA

E-mail: nahata@ece.utah.edu

New Journal of Physics 7 (2005) 249

Received 2 August 2005

Published 30 November 2005

Online at <http://www.njp.org/>

doi:10.1088/1367-2630/7/1/249

Abstract. Using terahertz (THz) time-domain techniques, we measure the relative coupling and scattering characteristics of surface plasmon-polariton waves for rectangular cross-section grooves on a thick metal foil. This is accomplished by using a single subwavelength aperture surrounded by one or more annular grooves. A unique aspect of the measurement technique is that it allows one to discriminate between the contributions of each groove in the transmitted THz waveform. The measurements are obtained by using structures that contain either a single annular groove, for coupling measurements, or two concentric annular grooves, for scattering measurements. The basic approach should be extendable to other spectral ranges and applicable to different forms of surface electromagnetic waves. Using the aforementioned measurements, we demonstrate the ability to alter the pulse shape of the transmitted waveform using a single aperture surrounded by four annular grooves of varying dimensions. In addition to the value of this capability for pulse shaping applications, the basic technique allows for greater control of the transmission resonance lineshape related to enhanced transmission through a single subwavelength aperture.

¹ Author to whom any correspondence should be addressed.

Contents

1. Introduction	2
2. Experimental details	3
3. Coupling and scattering of surface waves: experimental results and discussion	4
4. Application to pulse shaping and enhanced transmission	10
5. Conclusion	12
References	12

1. Introduction

Although surface waves at material interfaces, particularly surface plasmon-polaritons (SPP) at metal–dielectric interfaces, have been extensively studied over the last several decades [1], there appears to be resurgent interest in this topic [2]. This is driven largely by the ongoing desire to fabricate and examine structures of ever decreasing dimensions. An attractive feature of SPP fields is that they are strongly confined to the material interface and, at optical frequencies, typically extend less than a wavelength along the out-of-plane axis. Thus, the utilization of these bound waves may be well suited for a variety of nanophotonic applications. Several of the proposed and demonstrated applications include nanoscale guided wave devices [3, 4], optical switching [5], near-field photonics [6], enhanced nonlinear optical processes [7] and biosensors [8]. While the majority of the proposed devices have been designed for use at optical frequencies, there is growing interest in extending these ideas to significantly longer wavelengths, including the terahertz (THz) and microwave spectral ranges.

One application that is rarely discussed in the context of surface waves is that of pulse shaping. The ability to control arbitrarily the temporal and spectral properties of ultrafast pulses is of fundamental importance in a broad range of disciplines. Significant effort has been expended in recent years to create shaped femtosecond pulses at optical frequencies using a variety of spectral filtering techniques [9]–[11]. Such approaches have led to unique capabilities in the areas of high-speed communications, coherent control and spectroscopy. However, these approaches cannot be translated easily to ultrafast pulses in other regions of the electromagnetic spectrum. With specific regard to the far-infrared, several approaches have demonstrated the ability to generate freely propagating shaped THz pulses [12]–[15]. Such pulses may be applied to coherent control of molecular states, the study of linear and nonlinear carrier dynamics, and information coding in high-frequency optoelectronic devices. The ability to shape the temporal and spectral properties of surface propagating modes is expected to enhance and augment the capabilities available using current techniques. For example, in the case of high-frequency devices, information may be coded through appropriate shaping of THz pulses propagating along surface wave based guided-wave circuits. The pulse shaping process would need to be dynamically reconfigurable on a fast timescale for such an approach.

For the applications discussed above utilizing surface waves, including pulse shaping, there are two fundamental processes that must be carefully considered: the coupling efficiency of freely propagating radiation to propagating surface modes and the scattering characteristics induced by structures fabricated into the metal film on the surface waves. The traditional approaches to coupling radiation to surface wave modes typically rely on the use of prisms, gratings, or

near-field optical probes, since the propagation constant of the surface wave is usually larger than the corresponding free space propagation constant. These coupling techniques, as well as the subsequent surface wave propagation directions, have been extensively examined, both experimentally and theoretically [1, 16, 17]. Similarly, there have been countless theoretical and experimental studies investigating the scattering properties of surface waves under a wide variety of conditions, many of which date back over half a century. With the renewed interest in this research topic, there have been several recent studies examining the scattering efficiencies and propagation properties planar films with well-defined defects [18]–[22]. Of greater relevance to the present work are two experimental studies examining the coupling and scattering properties of rectangular cross-section grooves [23, 24]. However, since they use frequency domain techniques to analyse multiple periodically spaced grooves, it is difficult to separate the properties of these two processes.

In this submission, we characterize both the coupling of freely propagating THz pulses to surface waves and the scattering characteristics for these propagating waves on metal films containing rectangular cross-section grooves. The specific structure used in this study is based on a bullseye design, which comprises a single subwavelength aperture surrounded by one or more concentric annular grooves [23]. Using conventional THz time-domain techniques, we measure the transmitted THz waveform emitted through the aperture. As we have previously shown, this approach allows one to determine the contribution of each individual groove to the transmitted THz waveform [25]. Thus, the primary role of the aperture is to act as a local probe that simply samples the propagating surface wave. Based on the aforementioned measurements, we demonstrate a novel approach for THz pulse shaping. The technique relies not only upon the groove location, but also on the cross-sectional parameters of each individual annular groove. Although we show a simple proof-of-principle demonstration here, the technique may be used to create arbitrarily complex THz pulse shapes. An attractive feature of this approach is that the requisite structure can, in principle, be integrated directly into the potential application. It should be noted that while the present discussion will focus on the use of THz pulses to excite SPP, the basic approach should be extendable to other spectral ranges and applicable to different forms of surface electromagnetic waves.

2. Experimental details

We fabricated and analysed three separate sets of single aperture structures for the experimental studies mentioned above. Each bullseye pattern was fabricated by chemical etching on freestanding 150 μm thick stainless steel foils and consisted of a single 490 μm diameter circular aperture surrounded by one or more concentric annular grooves. In the first set of samples, designed to characterize the coupling properties, we fabricated 16 bullseye structures containing only a single annular groove surrounding the aperture with a centre-to-centre spacing of 3 mm. In seven of the structures, the groove width was fixed at 500 μm and the groove depth was varied from 0 to 100 μm . In the other nine structures, the groove depth was fixed at 100 μm and the groove width was varied from 0 to 800 μm . In the second set of samples, designed to characterize the scattering properties of the propagating surface waves, we fabricated 14 bullseye structures containing two annular grooves surrounding the aperture. The centre-to-centre spacing between the aperture and the first groove was 2 mm, while the centre-to-centre spacing between the first and second grooves was 2.75 mm. For all 14 structures, the outer groove was 100 μm deep and

500 μm wide. In five of the structures, the inner groove width was fixed at 500 μm and the groove depth was varied from 0 to 125 μm . In the other nine structures, the groove depth was fixed at 100 μm and the groove width was varied from 0 to 900 μm . Finally, in the third set of samples, designed to demonstrate pulse shaping capability, the bullseye patterns contained four annular grooves each. The groove-to-groove and aperture-to-inner groove spacing was 1 mm. The groove width was fixed at 500 μm , but the depth of each individual groove varied. For reference purposes, we fabricated 490 μm diameter bare apertures in the same metal foils.

We used a conventional time-domain THz spectroscopy setup [26] to characterize the structures discussed above. Details of the experimental setup and the advantageous properties of this approach have been previously discussed [25]–[27]. In all cases, the THz beam was incident on the corrugated surface at normal incidence. The nominal frequency content of the incident beam extends from ~ 0.05 THz ($\lambda = 6000$ μm) to ~ 1 THz ($\lambda = 300$ μm), with a peak frequency of ~ 0.3 THz ($\lambda = 1000$ μm).

3. Coupling and scattering of surface waves: experimental results and discussion

Figure 1(a) shows a representative photograph of a single annular groove bullseye structure used to characterize the coupling properties of the groove. As we have previously discussed, the transmitted time-domain waveform consists of two independent, yet phase-coherent, contributions: a contribution that arises from transmission of the incident THz pulse through the subwavelength aperture and a time-delayed contribution that arises from the interaction of the incident THz pulse with the structured metal film. These two components are shown schematically in figure 1(b) and the corresponding temporal waveforms are shown in figure 1(c). For each 1 mm spacing between the groove and the aperture, there is a 3.3 ps time delay between the initial bipolar waveform and the corresponding time-delayed oscillation. Given the bandwidth of the THz pulses used in this study, a groove-to-groove or groove-to-aperture spacing below approximately 0.6 mm would cause overlap between the associated time-domain pulses. If a smaller feature spacing is desired, higher bandwidth THz pulses are necessary in order to avoid an overlap between pulses. It is worth noting that while this specific bullseye structure and the drawings shown in figure 1 are similar to what we have previously presented [25], the nature of the measurements discussed here are fundamentally different than those discussed in our earlier study.

A quantitative determination of the absolute coupling efficiency related to the groove is not possible for several reasons. Firstly, the entire circular groove is excited by the incident THz beam. Preliminary results suggest that the circular grooves lead to a concentration of the surface electric field in the vicinity of the aperture, when compared to straight grooves. Secondly, the size of the subwavelength aperture is expected to strongly influence the sampling properties of the propagating surface wave. We are currently exploring this further. Finally, as we have previously discussed [25], the frequency content of the incident THz beam varies spatially, so the temporal properties of the THz pulse are also spatially dependent [28]. Thus, the incident beam properties are not expected to be identical at the aperture and the annular groove. Similar arguments hold for our inability to measure absolute scattering efficiencies.

In the measurements shown below, we are only able to measure relative coupling and scattering properties. In figure 1(c), the initial bipolar waveform (component A) is nominally identical to the transmitted THz time-domain waveform associated with a bare aperture. Although

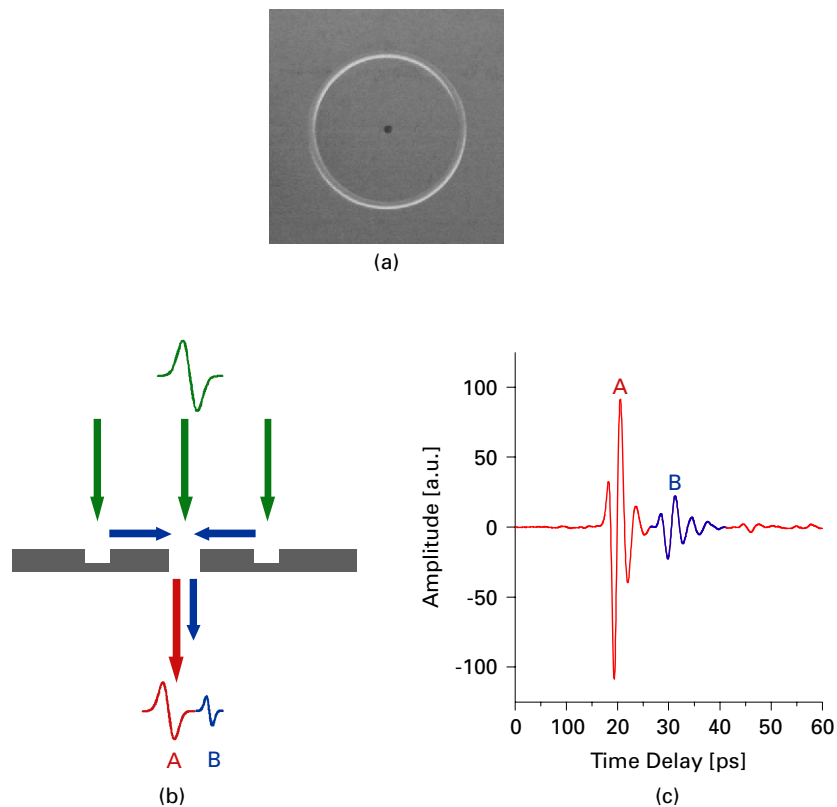


Figure 1. (a) Photograph of a typical bullseye structure consisting of only one annular groove. (b) Schematic drawing showing the two contributions to the transmitted THz time-domain waveform. The component shown by the red arrow corresponds to the non-resonant transmission of the incident THz pulse through the subwavelength aperture. The component shown by the blue arrow corresponds to the contribution that arises from the interaction of the incident THz pulse with the structured surface. (c) Measured time-domain waveform for structure in (a). The blue portion of the temporal waveform corresponds to the contribution that arises from coupling of the incident THz pulse by the annular groove (groove-to-aperture spacing is 3 mm).

the amplitude of this waveform component does not vary significantly, typically less than several per cent between all samples, we define the relative coupling efficiency as the ratio of normalized energy of the pulse B (figure 1(c)) to that of pulse A (figure 1(c)). The normalized energy is defined as the total spectrum energy divided by the central frequency, which is defined as the intensity weighted average frequency, for each wave component. If we ignore constants, the total spectrum energy, W , is defined as [29]

$$W_i \propto \int |E_i(\omega)|^2 d\omega, \quad (1)$$

where $|E(\omega)|$ is the magnitude of the THz electric field in the frequency domain, $i = A, B$ and corresponds to the wave component and ω is the THz radial frequency. The central frequency,

$\langle \omega \rangle$, is defined as [29]

$$\langle \omega \rangle_i = \frac{\int |E_i(\omega)|^2 \omega d\omega}{\int |E_i(\omega)|^2 d\omega}, \quad (2)$$

The relative coupling efficiency, RCE, given by

$$RCE = \frac{W_B / \langle \omega \rangle_B}{W_A / \langle \omega \rangle_A}, \quad (3)$$

may then be computed as a function of groove depth and width. It is worth noting that the central frequency, $\langle \omega \rangle$, is essentially identical for wave component B across each individual set of samples.

As discussed above, the transmitted time-domain THz waveform consists of two components: a temporal waveform containing the initial bipolar pulse that is nominally identical to the time-domain waveform of the bare aperture and an oscillation related to the coupling properties of the annular groove, shown in the blue trace in figure 1(c). The coupling efficiency is computed by numerically separating these two contributions. Figure 2(a) shows the relative coupling efficiency of a single annular groove for an incident broadband THz pulse. The groove width is fixed at $500 \mu\text{m}$ and the groove depth is varied between 0 and $100 \mu\text{m}$. The optimal groove depth appears to be $\sim 90 \mu\text{m}$ for the specific THz pulses used here. We plot the normalized amplitude spectra of waveform component B for three representative groove depths in figure 2(b). As may be seen from the figure, there is relatively little variation in the frequency content of the coupled THz beam over this wide range of groove depths. Figure 2(c) shows the relative coupling efficiency of a single annular groove for an incident broadband THz pulse as a function of the groove width. Here, the groove depth is fixed at $100 \mu\text{m}$ and the groove width is varied between 0 and $800 \mu\text{m}$. The optimal groove width appears to be $\sim 500 \mu\text{m}$ for the specific THz pulses used here. We numerically separate these two contributions to the time-domain waveform and plot the resulting normalized amplitude spectra of waveform component B for three representative groove widths in figure 2(d). Here again, there is only relatively minor variation in the frequency content of the coupled THz beam, although the differences are somewhat larger than observed when the groove depth is varied. Using these data, the optimal groove dimensions for maximum coupling appear to be $\sim 90 \mu\text{m}$ deep and $500 \mu\text{m}$ wide. This is consistent with our earlier observations [25, 27].

Next, we present data showing the effects of a surface wave traversing a rectangular cross-section groove. Figure 3(a) shows a representative photograph of a bullseye structure consisting of two annular grooves. Using these samples, we measure the relative transmission of a surface wave pulse coupled to the outer groove after traversing the inner groove. As was noted earlier, the aperture to inner groove distance of 2 mm was intentionally made different from the inner groove to outer groove distance of 2.75 mm, so as to minimize any potential resonant effects. The time-domain waveform consists of three components, as shown in figure 3(b): the initial bipolar waveform associated with the subwavelength aperture and two time-delayed oscillations related to the two annular grooves. These three contributions are highlighted in the corresponding temporal waveform shown in figure 3(c). In all of these samples, the cross-section of the outer groove is fixed. Thus, the surface wave oscillation coupled from this groove is nominally

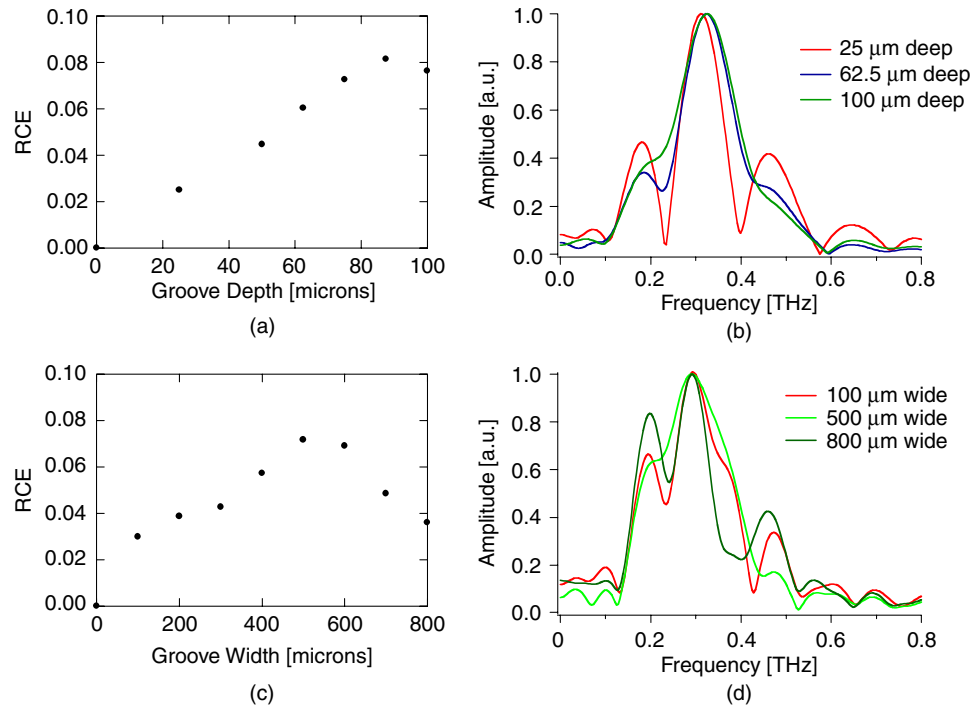


Figure 2. Dependence of relative coupling efficiency on groove cross-sectional parameters for a bullseye structure with only one annular groove. The relative coupling efficiency is measured as the ratio of the peak-to-peak amplitude of waveform component B (figure 1(c)) to the peak-to-peak amplitude of waveform component A (figure 1(c)). (a) Relative coupling efficiency versus groove depth. The groove width was fixed at 500 μm and the depth was varied from 0 to 100 μm in steps of 12.5 μm . Zero depth corresponds to a bare aperture. (b) Corresponding normalized amplitude spectra of waveform component B for three representative groove depths from (a). (c) Relative coupling efficiency versus groove width. The groove depth was fixed at 100 μm and the width was varied from 0 to 800 μm in steps of 100 μm . Zero width corresponds to a bare aperture. (d) Corresponding normalized amplitude spectra of waveform component B for three representative groove widths from (c).

identical from sample to sample. In order to characterize the relative transmission properties, we independently vary the depth and width of the inner groove and observe the change in the surface wave oscillation related to the outer groove (waveform C in figure 3(c)) after it traverses the inner groove. We compute a relative transmission efficiency in a manner similar to that shown for the computation of the relative coupling efficiency above. Using equations (1) and (2) above, we define the relative transmission efficiency, RTE, as

$$RTE = \frac{W_C / \langle \omega \rangle_C}{W_A / \langle \omega \rangle_A}, \quad (4)$$

where the subscript C in the numerator corresponds to waveform component C (figure 3(c)). As mentioned above, this measurement does not directly measure the scattering properties, but

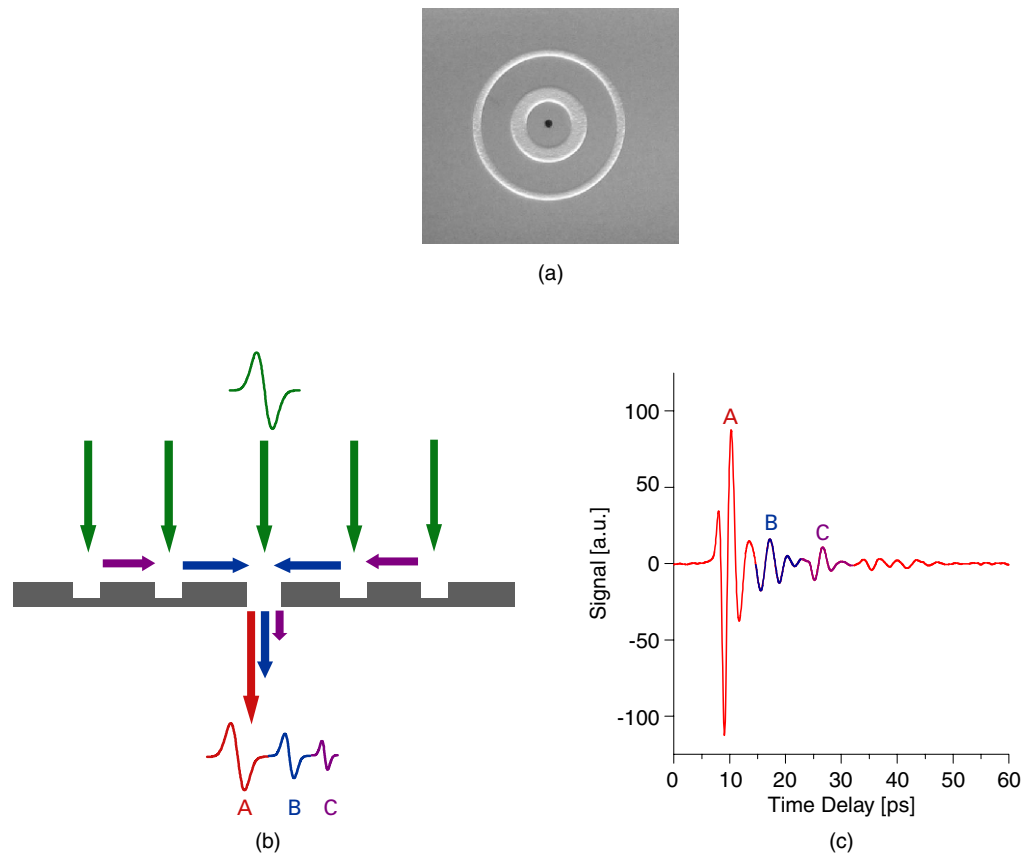


Figure 3. (a) Photograph of a typical bullseye structure consisting of only two annular grooves. (b) Schematic drawing showing the three contributions to the transmitted THz time-domain waveform. The component shown by the red arrow corresponds to the non-resonant transmission of the incident THz pulse through the subwavelength aperture. The components shown by the blue and purple arrows correspond to the contributions that arise from the interaction of the incident THz pulse with the structured surface. These latter components are smaller than the initial non-resonantly transmitted component and temporally delayed. (c) Measured time-domain waveform for structure in (a). The blue and purple portions of the temporal waveform correspond to the waveform components shown in (b). The inner groove-to-aperture spacing is 2 mm, while the outer groove to inner groove spacing is 2.75 mm.

rather the relative fraction of waveform C that is not scattered away from the forward propagation direction. Before discussing these results, it is worth noting that if we consider only the properties of waveform component B relative to waveform component A, as a function of width and depth, the results are consistent with the measurements discussed in figure 2.

Figure 4(a) shows the relative fraction of waveform C that is not scattered away from the forward propagation direction (relative transmission) as the depth of the inner groove is varied between 25 and 125 μm in 25 μm steps. Although the depth variation is comparatively large across the tested samples, the corresponding change in the relative amplitude of waveform component C is only $\sim 38\%$. After numerically separating the individual contributions to the

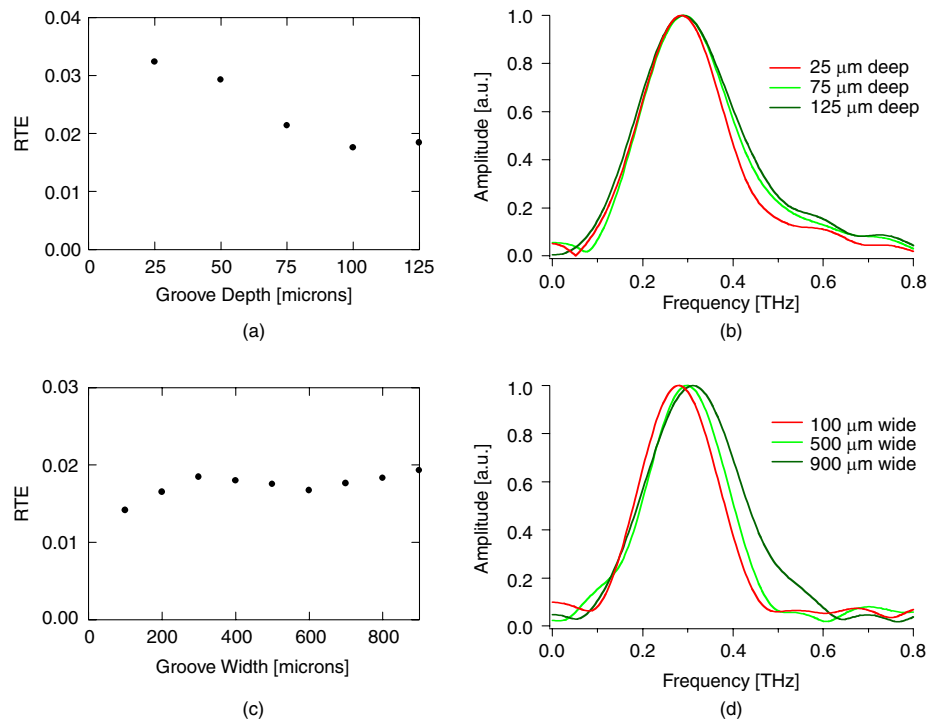


Figure 4. Dependence of relative transmission efficiency on groove cross-sectional parameters for a bullseye structure with two annular grooves. The outer groove cross-sectional parameters are fixed. The width and depth of the inner groove are varied. The relative transmission is measured as the ratio of the peak-to-peak amplitude of waveform component C (figure 3(c)) to the peak-to-peak amplitude of waveform component A (figure 3(c)). (a) Relative transmission versus depth of the inner groove. (b) Corresponding normalized amplitude spectra of waveform component C for three representative groove depths from (a). (c) Relative transmission versus depth of the inner groove. (d) Corresponding normalized amplitude spectra of waveform component C for three representative groove widths from (c).

time-domain waveform, we plot the resulting normalized amplitude spectra for waveform component C (see figure 3(c)) for three representative groove depths in figure 4(b). As observed earlier in figure 2(a), there is relatively minor variation in the frequency content of the forward propagating THz surface wave. Figure 4(c) shows the normalized fraction of waveform C that is not scattered away from the forward propagation direction as the width of the inner groove is varied between 100 and 900 μm in 100 μm steps. Here again, although the width variation is comparatively large across the tested samples, the corresponding change in the relative amplitude of waveform component C is only $\sim 15\%$. After numerically separating the individual contributions to the time-domain waveform, we plot the resulting normalized amplitude spectra for waveform component C (see figure 3(c)) for three representative groove widths in figure 4(d). There is relatively minor variation in the frequency content of the forward propagating THz surface wave, although it is more apparent than in figure 4(b). At this point, it is worthwhile to compare the experimental results presented here with relevant theoretical analyses. Of particular

interest is recent theoretical work by Sanchez-Gil and Maradudin, who have modelled the coupling and scattering properties of Gaussian and rectangular cross-section defects at optical frequencies [19]–[21]. We should note that making a direct comparison between these simulations and our experimental results is difficult for several reasons. Firstly, the dielectric properties of metals at optical and THz frequencies are very different. Also, the simulations yield absolute quantities, while the results presented here are only relative measurements. Nevertheless, we can compare general trends. Sanchez-Gil found that absolute coupling efficiencies increased as the groove width increased, for a fixed groove depth [19]. In contrast, we find that there is an optimal groove width for coupling of THz radiation. Beyond this optimal value, the coupling efficiency decreases. With regard to the scattering properties of these defects, the behaviour as a function of groove width can be rather complex. In the regime where the groove depth was small compared to the wavelength, Sanchez-Gil and Maradudin found that as the groove width increased, the defects acted as increasingly efficient light emitters [19]–[21]. The spectral properties of the transmitted THz waveforms peak at approximately 0.3 THz, corresponding to a free-space wavelength of 1 mm. For the measurements of the relative transmission efficiency as a function of groove width, the groove depth is 100 μm . Thus, the grooves examined here fall approximately within this regime of small normalized groove depth, suggesting that the relative transmission efficiency, RTE, should decrease with increasing groove width. This is exactly the opposite of what we observe. The reason for this discrepancy is not fully understood and requires further investigation. Given the broadband nature of the THz pulses, a full spatio-temporal description of the resulting travelling surface wave is necessary to understand its properties near the aperture. While such an analysis is highly desirable, it would require a complete three-dimensional numerical simulation and is beyond the scope of the present paper.

4. Application to pulse shaping and enhanced transmission

The bullseye structure examined here, along with associated structures such as a periodic array of subwavelength apertures, has been extensively examined for its enhanced transmission properties. Fundamental to the operation of these devices are the surface indentations that allow for both coupling and scattering of surface electromagnetic waves. Earlier, we mentioned the possibility of using such surface depressions fabricated into planar metal films for pulse shaping. In the present experimental geometry, ultrafast pulse shaping and enhanced transmission through subwavelength apertures are intricately linked. To demonstrate this, we consider the shaped THz pulse propagating along the metal surface. A fraction of this wave propagates through the aperture and is radiated into the far-field. By taking the Fourier transform of this transmitted temporal waveform, the transmission resonance lineshape in the frequency domain may be deduced [23, 25]. Using the coupling and scattering measurements shown in figures 2 and 4, we should be able to change the amplitudes of the individual time-delayed oscillations by altering the cross-sectional parameters of each groove.

In order to demonstrate this basic capability, we show a comparison of the transmitted THz waveform measured from two different bullseye structures in figure 5. Each of the patterns consisted of four-concentric annular grooves with a fixed width of 500 μm surrounding the subwavelength aperture, as shown in figure 5(a). One sample contains grooves of constant depth, while the other consisted of grooves of differing depth. For the bullseye structure with constant depth grooves, the amplitude of each oscillation is greater than that of the subsequent

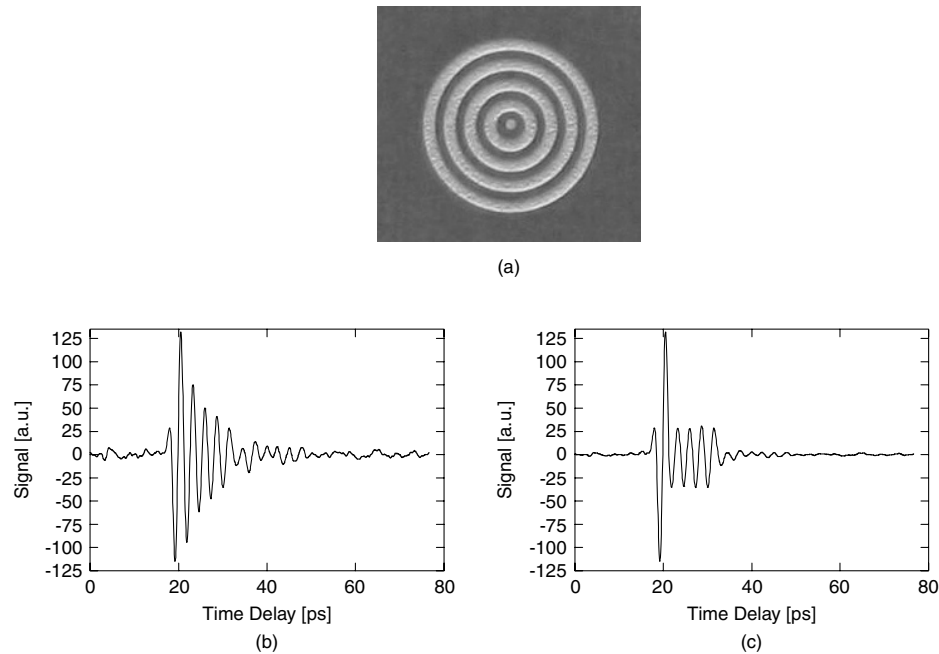


Figure 5. Demonstration of simple pulse shaping capability using bullseye structures of constant and varying groove depths. (a) Photograph of a typical bullseye structure consisting of four annular grooves. Only one photograph is shown since the two samples look very similar. (b) Experimentally observed time-domain waveform for bullseye structure consisting of a subwavelength aperture and four concentric annular grooves of identical cross-section ($100\ \mu\text{m}$ deep and $500\ \mu\text{m}$ wide). (c) Experimentally observed time-domain waveform for bullseye structure consisting of a subwavelength aperture and four concentric annular grooves with fixed width of $500\ \mu\text{m}$ wide and varying groove depths. Groove #1 is the innermost groove, while groove #4 is the outermost groove. The depths are: groove #1, $2.5\ \mu\text{m}$; groove #2, $37.5\ \mu\text{m}$; groove #3, $62.5\ \mu\text{m}$; groove #4, $100\ \mu\text{m}$.

time-delayed oscillation, as shown in figure 5(b). This is because the incident THz beam exhibits a Gaussian spatial profile with a relatively small beam diameter. With careful design of the groove parameters, it is possible to compensate for the non-uniform spatial profile of the beam, as we demonstrate in figure 5(c).

In order to demonstrate the basic procedure, consider the time-domain waveform in figure 5(b). The peak-to-peak amplitudes of the four oscillations are 190, 60, 45 and 34 for the first through fourth oscillations, respectively, in terms of the arbitrary y-axis units shown in figure 5(b). Since the groove depths are at the optimal value, the outer groove depths cannot be changed to increase the coupling efficiency and, thus, the corresponding oscillation amplitudes. However, the groove depths of the inner grooves can be reduced, so that their corresponding amplitudes are equal to that of the outer annular groove. It is important to note that when the depth of a groove is changed to alter its relative coupling efficiency, the relative transmission efficiency associated with this groove also changes. Thus, any change to a specific groove directly impacts the magnitude of the oscillations corresponding to the subsequent outer grooves. Beginning with the innermost groove, a reduction in its depth reduces the associated coupling factor. From

figure 4(a), it is apparent that there is also an increase in the corresponding relative transmission efficiency, causing an increase in the amplitudes associated with grooves two through four. Thus the depth of the second groove, relative to the aperture, would need to be reduced to compensate for this increase. This process can be extended to all of the grooves in the sample.

5. Conclusion

In conclusion, we have characterized both the coupling of freely propagating THz pulses to surface waves and the relative scattering efficiencies for these propagating waves on metal films containing rectangular cross-section grooves. The use of THz time-domain spectroscopy techniques allows us to uniquely determine the contribution of each individual groove to the transmitted THz waveform. Using the measured coupling and scattering parameters, we have demonstrated a novel approach for THz pulse shaping. The technique relies not only upon the groove location, but also on the cross-sectional parameters of each individual annular groove. We demonstrate a simple proof-of-principle experiment where the groove parameters are adjusted to compensate for the non-uniform spatial properties of the incident THz beam. In the present work, the centre-to-centre groove spacing was constant. In general, this is not a necessary requirement and the grooves may be arbitrarily positioned. This, combined with well-chosen groove cross-sectional parameters, should allow for the creation of arbitrarily complex temporal pulse shapes. Since the measurements described here are of the THz electric field, the frequency domain amplitude and phase spectrum, relevant to the transmission resonance lineshape, may be obtained by taking the Fourier transform. The approach further allows one to control the transmission resonance lineshape. The basic approach should be extendable to other spectral ranges and applicable to different forms of surface electromagnetic waves.

References

- [1] Raether H 1988 Surface plasmons on smooth and rough surfaces and on gratings (*Springer Tracts in Modern Physics* vol 111) (Berlin: Springer) and references therein
- [2] Barnes W L, Dereux A and Ebbesen T W 2003 Surface plasmon subwavelength optics *Nature* **424** 824–30
- [3] Burke J J, Stegeman G I and Tamir T 1986 Surface-polariton-like waves guided by thin, lossy metal films *Phys. Rev. B* **33** 5186–201
- [4] Charbonneau R, Berini P, Berolo E and Lisicka-Shrzek E 2000 Experimental observation of plasmon–polariton waves supported by a thin metal film of finite width *Opt. Lett.* **25** 844–6
- [5] Jung C, Yee S and Kuhn K 1994 Integrated optics waveguide modulator based on surface plasmon resonance *J. Light. Technol.* **12** 1802–6
- [6] Zayats A V and Smolyaninov I I 2003 Near-field photonics: surface plasmon polaritons and localized surface plasmons *J. Opt. A: Pure Appl. Opt.* **5** S16–S50
- [7] Nahata A, Linke R A, Ishi T and Ohashi K 2003 Enhanced nonlinear optical conversion using periodically nanostructured metal films *Opt. Lett.* **28** 423–5
- [8] Liu Y and Blair S 2003 Fluorescence enhancement from an array of subwavelength metal apertures *Opt. Lett.* **28** 507–9
- [9] Heritage J P, Weiner A M and Thurston R N 1985 Picosecond pulse shaping by spectral phase and amplitude manipulation *Opt. Lett.* **10** 609–11
- [10] Hillegas C W, Tull J X, Goswami D, Strickland D and Warren W S 1994 Femtosecond laser pulse shaping by use of microsecond radio-frequency pulses *Opt. Lett.* **19** 737–9

- [11] Weiner A M 1995 Femtosecond optical pulse shaping and processing *Prog. Quantum Electron.* **19** 161–237
- [12] Froberg N M, Hu B B, Zhang X-C and Auston D H 1991 Time-division multiplexing by a photoconducting antenna array *Appl. Phys. Lett.* **59** 3207–9
- [13] Liu Y, Park S-G and Weiner A M Terahertz waveform synthesis via optical pulse shaping 1996 *IEEE J. Quantum Electron.* **2** 709–19
- [14] Lee Y-S, Meade T, Perlin V, Winful H, Norris T B and Galvanauskas A 2000 Generation of narrow-band terahertz radiation via optical rectification of femtosecond pulses in periodically poled lithium niobate *Appl. Phys. Lett.* **76** 2505–7
- [15] Ahn J, Efimov A V, Averitt R D and Taylor A J 2003 Terahertz waveform synthesis via optical rectification of shaped ultrafast laser pulses *Opt. Express* **11** 2486–96
- [16] Otto A 1968 Excitation of nonradiative surface plasma waves in silver by the method of frustrated total reflection *Z. Phys.* **216** 398–410
- [17] Hecht B, Bielefeldt H, Novotny L, Inouye Y and Pohl D W 1996 Local excitation, scattering, and interference of surface plasmons *Phys. Rev. Lett.* **77** 1889–92
- [18] Pincemin F, Maradudin F A A, Boardman A D and Greffet J J 1994 Scattering of a surface plasmon polariton by a surface defect *Phys. Rev. B* **50** 15261–75
- [19] Sanchez-Gil J A 1998 Surface defect scattering of surface plasmon polaritons: mirrors and light emitters *Appl. Phys. Lett.* **73** 3509–11
- [20] Sanchez-Gil J A and Maradudin A A 1999 Near-field and far-field scattering of surface plasmon polaritons by one-dimensional surface defects *Phys. Rev. B* **60** 8359–67
- [21] Sanchez-Gil J A and Maradudin A A 2004 Dynamic near-field calculations of surface-plasmon polariton pulses resonantly scattered at sub-micron metal defects *Opt. Express* **12** 883–94
- [22] Rivas J G, Kuttge M, Bolivar P H and Kurz H 2004 Propagation of surface plasmon polaritons on semiconductor gratings *Phys. Rev. Lett.* **93** 256804/1–4
- [23] Thio T, Pellerin K M, Linke R A, Lezec H J and Ebbesen T W 2001 Enhanced light transmission through a single subwavelength aperture *Opt. Lett.* **26** 1972–4
- [24] Lockyear M J, Hibbins A P, Sambles J R and Lawrence C R 2005 Enhanced microwave transmission through a single subwavelength aperture surrounded by concentric grooves *J. Opt. A: Pure Appl. Opt.* **7** S152–S158
- [25] Agrawal A, Cao H and Nahata A 2005 Time-domain analysis of enhanced transmission through a single subwavelength aperture *Opt. Express* **13** 3535–42
- [26] Grischkowsky D 1992 *Frontiers in Nonlinear Optics* ed H Walther, N Koroteev and M O Scully (Bristol: Institute of Physics Publishing) and references therein
- [27] Cao H, Agrawal A and Nahata A 2005 Controlling the transmission resonance lineshape of a single subwavelength aperture *Opt. Express* **13** 763–9
- [28] Feng S, Winful H G and Hellwarth R W 1998 Gouy shift and temporal reshaping of focused single-cycle electromagnetic pulses *Opt. Lett.* **23** 385–7
- [29] Diels J C and Rudolph W 1996 *Ultrashort Laser Pulse Phenomena: Fundamentals, Techniques, and Applications on a Femtosecond Time Scale* (San Diego, CA: Academic) pp 12–15